



# Thermodynamic, kinetic and equilibrium isotherm studies of As(V) adsorption by Fe(III)-impregnated bentonite

Shima Barakan<sup>1</sup> · Valeh Aghazadeh<sup>1</sup> · Abdoullah Samiee Beyragh<sup>2</sup> · Sahar Mohammadi<sup>1</sup>

Received: 1 September 2018 / Accepted: 16 July 2019 / Published online: 22 July 2019  
© Springer Nature B.V. 2019

## Abstract

Arsenic removal has received much attention all over the world because of its toxicity and carcinogenicity. In the current research, the adsorption behavior of As(V) from aqueous solution onto Fe(III)-impregnated bentonite (Fe-Bent) was examined. Adsorption experiment results showed that the adsorption capacity of initial bentonite clay (Bent) was increased by Fe(III)-impregnation method. In Fe-Bent, the mononuclear Fe(III) cations, small oligomeric cluster and bulky  $Fe_xO_y$  particles were made such active sites identified by UV–Vis spectroscopy. X-ray diffraction results showed that Fe(III) species presented mainly in both crystalline and amorphous forms on the external surface of Fe-Bent. In an experimental study, the effect of different parameters such as contact times, arsenic concentrations, adsorbent dosages, pH and temperature conditions was investigated. Fe-Bent sample represented the maximum adsorption capacity of  $10.06 \text{ mg L}^{-1}$  to remove  $5\text{--}20 \text{ mg L}^{-1}$  of As(V) at  $\text{pH}=6$  and ambient temperature. In this experiment, the residual As(V) concentration decreased to less than  $0.01 \text{ mg/L}$  with the adsorption efficiency of 99% (i.e., below the limit of the WHO). The two- and three-parameter isotherm models revealed the best fit to the Freundlich, Sips, Toth, Temkin and Langmuir models, respectively. The isotherm models indicated the strong adsorption between arsenic and Fe-Bent. The adsorption kinetics was also considered by first-order, second-order and Elovich rate equations. It was noticed that the Fe-Bent adsorption followed the external surface reaction such as ligand exchange and surface complexation. The thermodynamics studies exposed that the process was spontaneous and endothermic for Fe-Bent.

**Keywords** Adsorption · Impregnated bentonite · Arsenic · Thermodynamics · Kinetics · Isotherm

---

✉ Valeh Aghazadeh  
v.aghazadeh@sut.ac.ir

Extended author information available on the last page of the article

## 1 Introduction

Arsenic is mostly found in trivalent and pentavalent oxidation states in natural water systems. Redox potential is the main factor for controlling the arsenic species. The  $\text{H}_2\text{AsO}_4^-$  is the dominant species under oxidizing conditions at pH less than 6.9, while  $\text{HAsO}_4^{2-}$  is dominant at higher pH. The  $\text{H}_3\text{AsO}_3$  becomes dominant under reducing conditions at pH less than 9.2 (Chiban et al. 2012). Exposure to arsenic can cause a variety of unfavorable health effects. The world health organization (WHO) recommended  $0.01 \text{ mg L}^{-1}$  as a guideline value for arsenic in drinking water (Yamamura et al. 2003).

Many conventional and non-conventional methods have been employed for arsenic removal. Adsorption method is applied widely to remove arsenic metal from wastewater and effluent. The low cost, easy operation, availability and efficiency are the significant advantages of adsorption. In comparison with conventional methods, e.g., ion exchange resin, filtration and membrane technology, adsorption is an economic and environmentally friendly (Langsch et al. 2012). The iron hydroxide/oxide (Fazi et al. 2016; Sigdel et al. 2016; Prathna et al. 2017; Polowczyk et al. 2018) and iron-based composites such as the Mg–Fe-based hydrotalcites (Türk et al. 2009) and Fe-hydrotalcite supported magnetite nanoparticle (Türk and Alp 2014) as the layered double hydroxide (LDH) adsorbents were investigated by high removal efficiency of As(V) under the WHO limit value. Moreover, the activated alumina (Chen et al. 2014) and activated carbon–iron oxide (Oliveira et al. 2002) have been studied several times for adsorption processes. In this way, limited studies have been focused on the arsenic adsorption by clay minerals due to a large amount of negative surface charge with low affinity for arsenic removal (Jovanović et al. 2011; Uddin 2017). Clay minerals have attracted significant attention due to their high abundance, environmental compatibility, low cost, operation simplicity, easy availability and reusability. The swelling capacity, cation exchange capacity, textural structures and surface acidity properties make clays attractive for various applications in adsorption and catalysis process (Mohan and Pittman 2007). The pH-dependent charges in bentonite clay minerals are effective adsorbents for cationic, anionic and neutral species (Mohan and Pittman 2007). Therefore, bentonite could be used as an inexpensive arsenic adsorbent in agricultural and industrial wastewater (Ranjan et al. 2009). In this way, the surface modification of clay minerals is considered as an attractive way to increase their adsorption capacity for pollution control. The favored groups of substances for arsenic removal are iron compounds, including hematite, goethite, granular ferric hydroxide and iron oxide-coated materials. The mechanism of arsenic adsorption has been assigned to ligand exchange reaction, surface complexation by specific adsorption to surface hydroxyl groups and co-precipitation (Nayak and Singh 2007).

Adsorption of arsenic from aqueous solution with iron modified kaolinite, illite and montmorillonite have been investigated (Mohapatra et al. 2007). The tendency for As(V) adsorption was reported greater than As(III) on kaolinite and montmorillonite in acidic condition, while, at pH values above 7, As(III) adsorption was usually greater than As(V) adsorption (Goldberg and Johnston 2001).

This paper deals with the possible application of Fe(III) impregnation method to prepare Fe-Bent with several iron oxides active sites. Fe-Bent was used for adsorption of inorganic arsenic from aqueous solution to access the lower amount of arsenic residual in the WHO limit value of  $0.01 \text{ mg L}^{-1}$ . This research was also focused on the Fe-Bent in the various experimental conditions to remove As(V). The arsenic removal

mechanisms were revealed by different two- and three-parameter isotherm models. Furthermore, the thermodynamics and kinetics of As(V) adsorption onto Fe-Bent were studied.

## 2 Experimental

### 2.1 Materials

Natural bentonite was obtained from Shahrood mining company, Semnan, Iran.  $\text{FeCl}_3 \cdot 6\text{H}_2\text{O}$  (Merck Co),  $\text{NaCl}$  (Merck Co),  $\text{AgNO}_3$  (Merc. Co) and  $\text{Na}_2\text{AsO}_4 \cdot 7\text{H}_2\text{O}$  (Titra-Chem Co.) were used to modify bentonite, and to prepare adsorbate solution.

### 2.2 Methods

For the preparation of Fe-Bent, the natural bentonite was purified in the laboratory. Dispersion, Na-activation, sedimentation based on the Stokes' Law, sonication and centrifugation methods were used to remove quartz, organic matter and carbonates. The purified sample was ground and sieved through 325 mesh. To obtain  $\text{Na}^+$ -exchanged bentonite, the purified bentonite added in 1.0 M  $\text{NaCl}$  at a ratio of S:L = 1:100 (w/w) at 80 °C for 2 h in three times (Timofeeva et al. 2009). It was then washed to remove chloride by the  $\text{AgNO}_3$  test (Yan et al. 2008). To prepare Fe-Bent, 300 g of Na-bentonite was added into a 1000-mL beaker filled with 0.1 M  $\text{FeCl}_3 \cdot 6\text{H}_2\text{O}$  solution in pH=2. The beaker was placed on a magnetic stirrer for 12 h at 85 °C. Then, the sample was baked on a hot plate at 150 °C for 6 h. To remove uncoated soluble iron, the baked Fe-Bent was washed and dried at 105 °C. The schematic of the impregnation method is shown in Fig. 1.

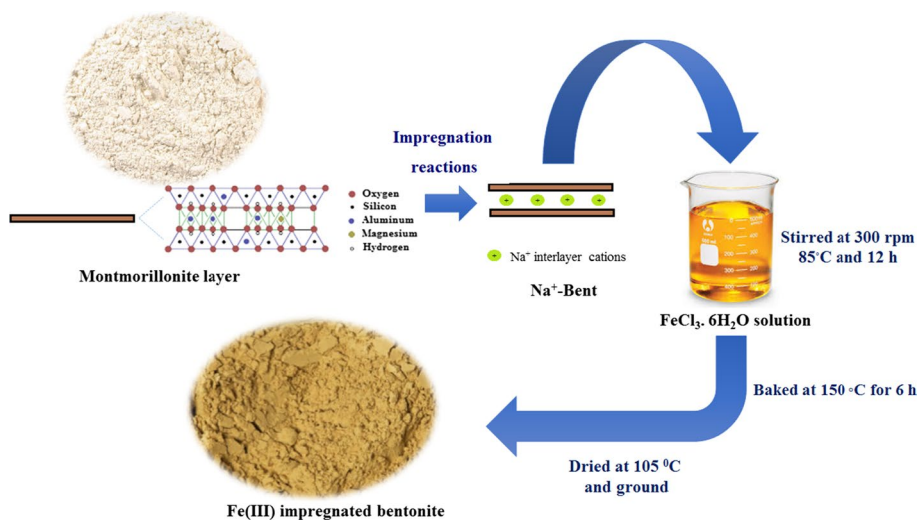


Fig. 1 Schematic of impregnation method to the synthesis of Fe-Bent

The stock solution (1000 mg L<sup>-1</sup> As(V) concentration) was prepared by dissolution of Na<sub>2</sub>HAsO<sub>4</sub>·7H<sub>2</sub>O salt in de-ionized water. Then, the dilution of the stock solution was done to prepare different As(V) concentrations (5–20 mg L<sup>-1</sup>).

### 2.3 Characterization techniques

N<sub>2</sub> adsorption–desorption was used at –196 °C using a specific surface area and porosity analyzer Belsorp mini. The Brunauer–Emmett–Teller (BET) method was used to determine the specific surface area of Bent and Fe-Bent. The total pore volume ( $V_t$ ) was calculated from the amount of nitrogen adsorbed at a relative pressure of 0.99. The  $t$  plot method was used to determine the total micropore volume ( $V_{mic}$ ,  $t$ ) and the specific surface area of micropores ( $S_{mic}$ ,  $t$ ) and mesopores ( $S_{mes}$ ,  $t$ ). The pore size distributions and mesopore volume ( $V_{mes}$ ) were determined by BJH methods. The XRD analysis of none modified Bent and Fe-Bent samples was done with a Philips X’Pert Pro instrument (Cu K $\alpha$  radiation) in the range of  $2\theta=4^\circ$ – $80^\circ$ ; also to determine the chemical compositions of Bent and Fe-Bent the XRF analysis was used by ARL 9400 XP+ spectrometer (voltage 20–60 kV). To determine the functional groups for Bent and Fe-Bent, the FTIR spectra were recorded in the range of 400–4000 cm<sup>-1</sup> on a Bruker Vertex 70 spectrophotometer. The structural morphology of Bent and Fe-Bent was analyzed by scanning electronic microscopy (SEM, Philips XL-30), and the elemental compositions were measured by semi-quantitative energy dispersive X-ray techniques (EDX). To identify the nature of iron species, iron amounts and their distribution onto the bentonite, the UV–Vis spectroscopy (T110+ double monochromator UV–visible spectrophotometer) was used in the absorbance range of 180–600 nm. The arsenic concentration in the adsorption experiments was measured by ICP-mass spectrometry (ICP-MS, Elan 6000 DRC). To determine cation exchange capacity (CEC), the Bower method (Bower et al. 1952) was used for Bent and Fe-Bent samples. The flame photometer device (360, Sherwood) was also used for Na<sup>+</sup>, Ca<sup>2+</sup> and K<sup>+</sup> measurements in CEC method. In this research, the planetary ball mill (p6, Fritsch) carried out for crushing and grinding of dried bentonite.

### 2.4 The pH<sub>zpc</sub> determination method

pH<sub>zpc</sub> is the pH of zero point charge (Weber and DiGiano 1996). To estimate the effect of pH in the adsorption process, the pH<sub>zpc</sub> of the Bent and Fe-Bent was determined in the batch equilibrium system. In this way, the 1:100 (solid/liquid) ratio of the 0.01 M NaCl solution was prepared as the inert electrolyte. Then, the 0.5 g of each sample was mixed by 40 mL of NaCl electrolyte in the initial pH ranges between 2 and 12. To measure the final pH values, the equilibrium time reached after 48 h (Labinco, L82). Finally, the plot of  $\Delta$ pH versus initial pH value indicated the pH<sub>zpc</sub> at  $\Delta$ pH = 0 (Gitari 2014).

### 2.5 Batch experiment

To investigate the arsenic adsorption, the effect of As(V) concentration, pH, contact time and bentonite dosage was evaluated. Batch adsorption experiments were performed at 298, 308 and 318 K. 0.01, 0.05, 0.1 and 0.5 g of natural and modified bentonite were added into the 100-mL flasks containing 50 mL solution with various concentrations of As(V) between 5 and 20 mg L<sup>-1</sup>. The pH of solution was adjusted in different pH ranges from 2 to

8 by adding amounts of 1 M NaOH or 1 M HCl, and the bottles were shaken by a magnetic stirrer for 5, 30, 60, 120, 180 and 240 min to attain equilibrium. Then, the supernatant was filtered, and the arsenic concentration was measured using ICP-MS. The arsenic removal efficiency and the equilibrium arsenic adsorption capacity for adsorbent were determined, respectively, by Eqs. (1) and (2).

$$R = \frac{C_0 - C_e}{C_0} \times 100 \quad (1)$$

$$q_e = (C_0 - C_e) \times \frac{V}{M} \quad (2)$$

## 2.6 Measurement of the iron content stability

In this study, the acidic leaching was chosen to estimate the stability of iron contents (Lu 1995). 0.03 g of Fe-Bent was added into the 30 mL beaker with 1:1 HCl solution, and the beaker was shaken by magnetic stirrer at 500 rpm for 10 h. Then, the beaker was set in a heater stirrer at 80 °C for 4 h. Finally, the Fe-Bent was filtered and the iron concentration in the supernatant was analyzed by UV-Vis spectra. The iron content was calculated according to Eq. (3).

$$\text{Iron content} = \frac{\text{Mass of iron}}{\text{Mass of bentonite} + \text{mass of iron}} \times 100. \quad (3)$$

## 3 Results and discussions

### 3.1 Composition and characteristics of adsorbents

On the basis of pHzpc measurement results, the increase in pHzpc after the modification was evidenced in Fe-Bent. The presence of Fe(III) ions on the external surface and the edge of Fe-Bent may cause this increment. The pHzpc for bentonite was 4.9. After modification,

**Fig. 2** Deconvoluted UV-Vis spectrum received from the Fe-Bent

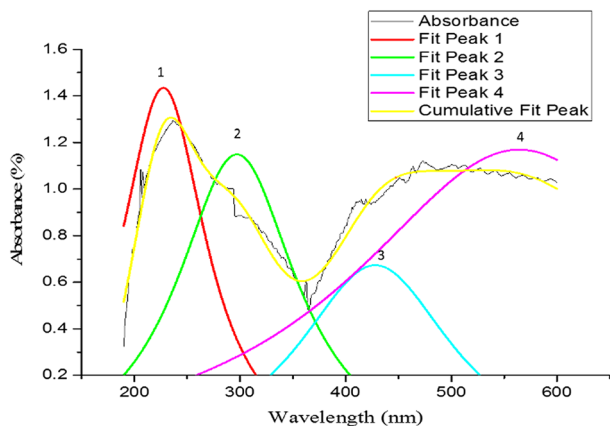


**Table 1** Deconvoluted UV-Vis spectrum data for Fe-Bent

Plot	Lorentz			
	Peak 1 (absorbance)	Peak 2 (absorbance)	Peak 3 (absorbance)	Peak 4 (absorbance)
Wavelength ( $\text{cm}^{-1}$ )	227.53007 $\pm$ 3.34589	297.13198 $\pm$ 38.33399	427.9642 $\pm$ 30.6457	564.2592 $\pm$ 23.40238
Iron species	Tetrahedral mononuclear Fe(III) cations	Octahedral mononuclear Fe(III) cations	Small oligomeric $\text{Fe}_x\text{O}_y$ cluster	Bulky $\text{Fe}_x\text{O}_y$ particles
Reduced Chi-square	0.0014			
$R^2$	0.98			

the pHzpc changed to 8.3. Therefore, Fe-Bent has a positive charge for  $\text{pH} < 8.3$  and shows a negative charge for  $\text{pH} > 8.3$ .

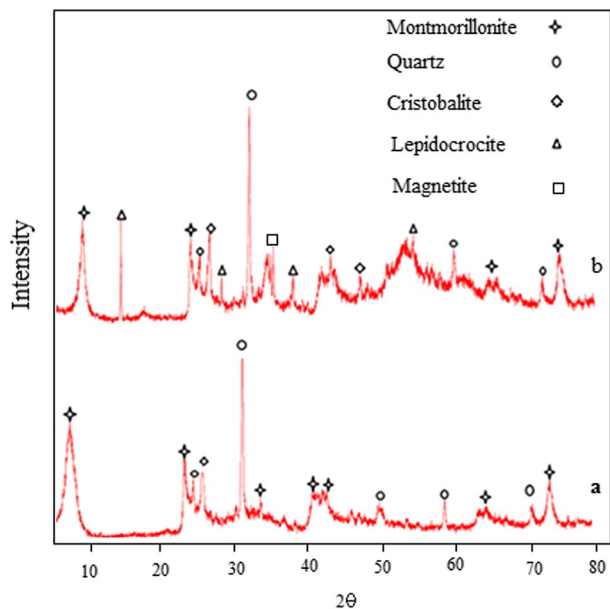
The UV–Vis spectra were deconvoluted in the wavelength range 190–600 nm by OriginPro in Lorentz model. As shown in Fig. 2 and Table 1, four peaks in Fe-Bent UV–Vis spectra represent the presence of different species of iron (III) ions. Moreover, the UV–Vis spectra give information about the coordination of the iron species. The ligand (oxygen)-to-metal charge transfer is attributed to O–Fe charge transfer transitions observed at 240–300 nm. Bands at ca. 400–500 nm are ascribed to the extra-framework Fe(III) ions due to medium intense  $d-d$  electron pair transition. The bands larger than 500 nm correspond to larger particles formed of  $\text{Fe}_x\text{O}_y$  (Liu et al. 2015). Accordingly, various active sites at Fe-Bent were made by the mononuclear  $\text{Fe}^{3+}$  cations, small oligonuclear  $\text{Fe}_x\text{O}_y$  clusters and bulky particles of  $\text{Fe}_2\text{O}_3$ .

The physical and chemical analysis of Fe-Bent and Bent is carried out with the intense  $d_{001}$  reflections observed at  $8.34^\circ$  and  $6.04^\circ$  in the basal spacing of 10.60 Å and 14.60 Å, respectively. In Fig. 3, the XRD pattern shows that the montmorillonite with the JCPDS file number of 96-900-0960 is the main compound. Before modification, the major impurities in the bentonite structure include the quartz and cristobalite with the JCPDS file number of 96-900-7287 and 96-900-1581, respectively. After Fe-impregnation methods, the XRD pattern shows the composite material in both crystalline and amorphous species in Fe-Bent. The presence of  $\gamma$ -FeOOH (lepidocrocite) and  $\text{Fe}_3\text{O}_4$  (magnetite) with JCPDS file number of 96-101-1027 and 96-900-5638 is indicated by the major reflection at  $2\theta = 15^\circ$  and  $35^\circ$ , respectively.

As shown in Fig. 3, the decrease in  $d_{001}$  values can be corresponded to the leaching and partial protonation of the interlayer cations in Fe-Bent (Krupskaya et al. 2017).

FTIR spectra of Bent and Fe-Bent are presented in Fig. 4. The peaks corresponding to the Al–Mg–OH and Al–Al–OH stretching vibrations resulting from octahedral sheets of bentonite clay were located at  $3630\text{--}3625\text{ cm}^{-1}$  (Putra et al. 2009). The O–H stretching

**Fig. 3** XRD patterns of **a** Bent and **b** Fe-Bent



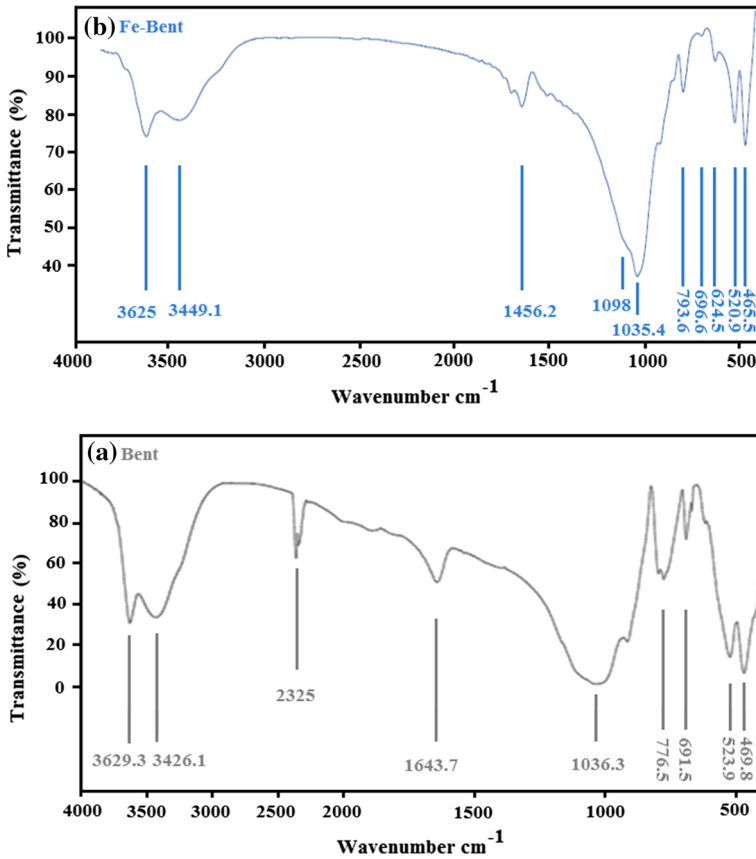


Fig. 4 FTIR spectra of **a** Bent and **b** Fe-Bent

vibration of the structural hydroxyl groups and the water molecules presented in the inter-layer were observed at 3449–3426  $\text{cm}^{-1}$  (Abukhadra et al. 2018b). The H–O–H deformation band of water molecule was observed at 1632–1620  $\text{cm}^{-1}$ . The H–O–H stretching vibration of the adsorbed water molecule was shown at 2325  $\text{cm}^{-1}$ . The observation peaks corresponding to Si–O–Si stretching and Si–O bending vibrations were observed at 1035 and 465  $\text{cm}^{-1}$ , respectively. The Si–O vibration band corresponding to quartz, silica and cristobalite was shown at 793  $\text{cm}^{-1}$ , 696 and 691  $\text{cm}^{-1}$ , respectively. Therefore, all of the bands corresponding to the bentonite structure were retained in all of the Bent and Fe-Bent samples, indicating that the structural damage of bentonite was not happened by the impregnation method.

In Fe-Bent spectra, the intensity of OH vibration band decreased due to the baking process in the impregnation method. Moreover, in Fe-Bent, the observation of the new peaks at 470 and 1098  $\text{cm}^{-1}$  was assigned to the lepidocrocite/magnetite phases (Pradisty et al. 2017), and iron hydroxo complexes (e.g., Fe–OH and Fe–OH–Fe), respectively (Devi et al. 2014).

As shown in Fig. 5, the SEM–EDX analysis of Bent and Fe-Bent samples gives helpful information on the distribution of Fe(III) ions in the structure of bentonite. The



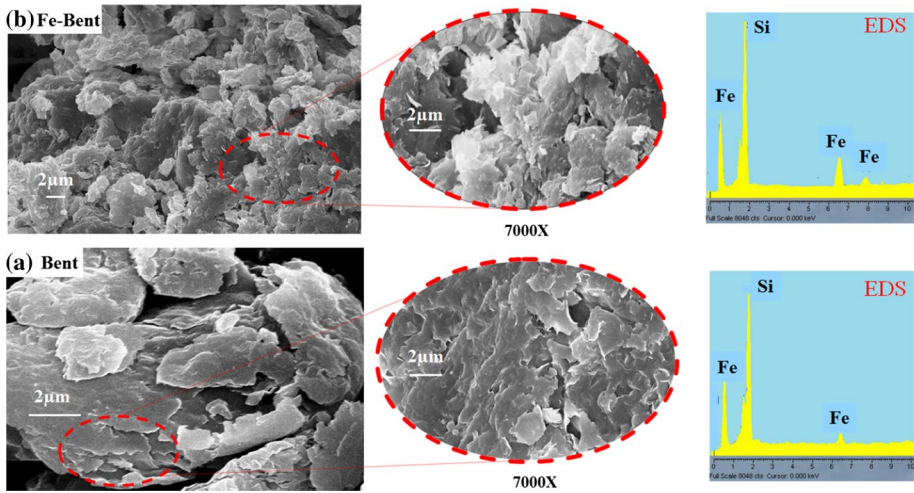


Fig. 5 SEM-EDX images of a Bent and b Fe-Bent

Table 2 N<sub>2</sub> adsorption–desorption results of Bent and Fe-Bent

Sample	$S_{BET}$ (m <sup>2</sup> /g)	$S_{mic,t}$ (m <sup>2</sup> /g)	$S_{mes,t}$ (m <sup>2</sup> /g)	$V_{mic,t}$ (cm <sup>3</sup> /g)	$V_{total}$ (cm <sup>3</sup> /g)	$V_{mes}$ (cm <sup>3</sup> /g)	$D_a$ (nm)
Bent	28	28.06	18.49	0.004	0.10	0.09	19.90
Fe-Bent	168	79.50	73.96	0.17	0.19	0.01	10.07

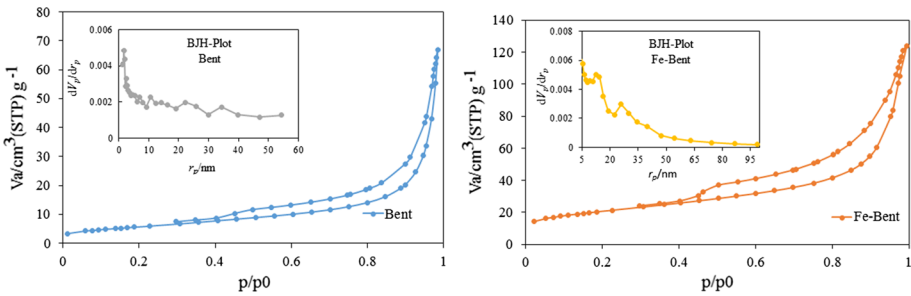


Fig. 6 Adsorption–desorption isotherms and the corresponding pore size distribution (inset) of Bent and Fe-Bent

Bent is composed of the large flaky particles, while the Fe-Bent shows small particles related to the probable presence of Fe(III) ions without any destructive effect for basic clay layer. This property was also verified by EDX analysis. The results show a rather increase in the amount of Fe(III) ions on the external surface of Fe-Bent, which causes to increase the adsorption efficiency of Fe-Bent. The main mechanism of Fe(III) ions distribution probably belongs to tack place Fe(III) ions in an external surface of bentonite or ferric precipitates on the internal surface of bentonite. In addition, the modification of bentonite shows the homogeneous pore sizes in the morphologies of Fe-Bent.

**Table 3** XRF analysis of bentonite before and after Fe-modification

Element/composition	Fe-Ben (wt%)	Bent (wt%)
SiO <sub>2</sub>	46.00	52.38
Al <sub>2</sub> O <sub>3</sub>	17.91	15.27
Fe	8.10	4.08
CaO	0.29	4.07
Cl	0.16	1.56
MgO	1.92	6.37
SO <sub>3</sub>	0.56	4.68
P <sub>2</sub> O <sub>5</sub>	0.08	0.23
LOI	33.35	11.31

The obtained results from N<sub>2</sub> adsorption–desorption for Bent and Fe-Bent are shown in Table 2 and Fig. 6. These results revealed that the Fe(III) impregnation method in bentonite clay increased the BET surface area from 28 to 168 m<sup>2</sup>/g. This aspect could be depended on the formation of different iron species active sites on Fe-Bent. The presence of iron particles increased the micropores volume and total pore volume. According to IUPAC (International Union of Pure and Applied Chemistry) classification, the Bent and Fe-Bent showed the isotherms assigned to type IV with H4 hysteresis loop. H4 indicated the formation of narrow slit-like pores. Therefore, the large BET surface area, the increase in micropores volume and the decrease in mean pore diameter (Da) corresponded to Fe(III) impregnated bentonite. As shown in Fig. 6, the pore size distribution of Fe-Bent was more homogenous than Bent with several peaks.

The other physical properties of clay mineral include CEC. The CEC of bentonite after Na-activation by NaCl salt is changed from 117 to 124 meq/100 g clay. This feature helps bentonite to have a high capacity for cation exchange in the impregnation method.

According to the XRF results, the chemical compositions of bentonite before and after modification are shown in Table 3. The amount of Fe(III) ions after modification increased from 4.08 to 8.10 wt%. The impurities of initial bentonite were relatively decreased, and its quality was much increased by a large amount of Fe content.

### 3.2 Iron content of adsorbents

The stability of iron was measured at pH=2 due to the iron content dissolution of Fe-Bent under acidic conditions. The Fe content of Fe-Bent was analyzed by UV–Vis spectroscopy after acidic leaching. In this pH for 1 g L<sup>-1</sup> of bentonite, the iron concentration was achieved about 16 mg L<sup>-1</sup> which was equaled to 40% of the impregnated iron content. Therefore, this adsorbent revealed a high capacity for As(V) removal. The results showed that the adsorbent was modified well. Moreover, the Fe-Bent could be applied on acidic effluent (e.g., acid mine dragging in mine wastewater).

### 3.3 Effect of adsorbent dosage

In the adsorption experiment, the effect of Bent and Fe-Bent dosages was studied on the range of 0.01, 0.05, 0.1 and 0.5 g. For this purpose, all samples were mixed to 50 mL of arsenic solution with a concentration of 10 mg L<sup>-1</sup> at pH=6. Then, these mixtures were stirred at

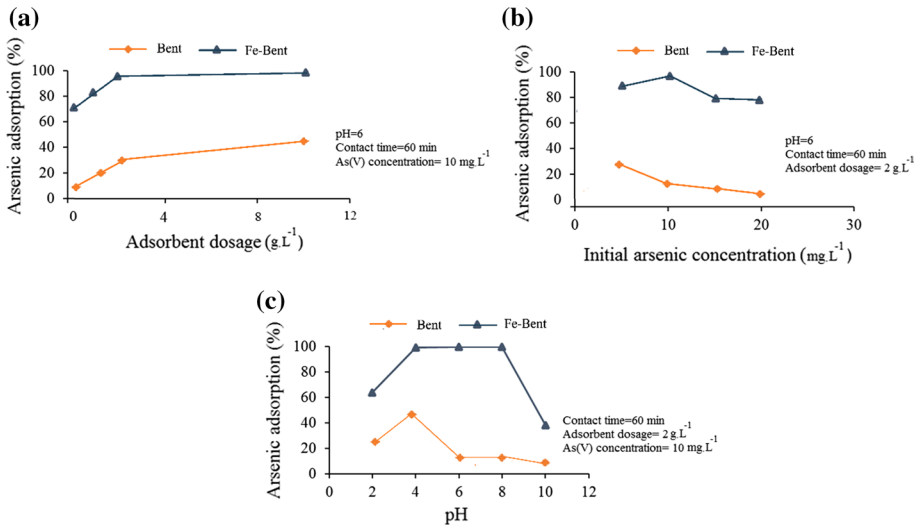


**Fig. 7** Effect of **a** adsorbent dosages, **b** arsenic concentration and **c** pH on the arsenic adsorption from aqueous solution for Bent and Fe-Bent

300 rpm for 60 min at ambient temperature. Finally, the Bent and Fe-Bent were separated from the solution and the concentration of arsenic was evaluated by ICP-MS.

As shown in Fig. 7a, the increase in Fe-Bent dosage distinctly decreased the amount of arsenic in solution at the beginning, and then, it was obtained the maximum decreasing due to the high available adsorption sites and high surface contact for the adsorption process. The dosage of 2 g L<sup>-1</sup> for Fe-Bent was taken as the optimum dosage with removal percentage of 99%. After that, the extra addition of the Fe-Bent caused the saturation and the removal efficiency of the adsorbent decreased. In the Bent, the amount of As(V) adsorbed increased up to 43% in the dosage of 10 g L<sup>-1</sup>. Therefore, Bent showed lower adsorption efficiency than Fe-Bent.

### 3.4 Effect of arsenic concentration

The effect of arsenic concentration in the adsorption process was studied under various concentration from 5 to 20 mg L<sup>-1</sup> with 2 g L<sup>-1</sup> of adsorbent dosage, at pH=6 and ambient temperature. As shown in Fig. 7b, the Fe-Bent was more suitable adsorbent at As(V) concentrations of 10 mg L<sup>-1</sup> with removal percentage of 99%. At higher concentrations of As(V), the adsorption efficiency reduced due to the decrease in available active sites. In the Bent sample, As(V) adsorption was favored at the concentrations of 5 mg L<sup>-1</sup> with the efficiency of 31% and then drastically decreased.

### 3.5 Effect of pH

The arsenic adsorption from aqueous solution using Bent and Fe-Bent was shown the extremely pH-dependent process. The pH of the solution indicated the interaction between physicochemical properties of arsenic ion species and the surface charge of the adsorbent. In the pH ranges from 2 to 10, the adsorption behavior of As(V) ions was

**Table 4** Isotherm models equations with two and three parameters

	Equations
Isotherm models	Two parameters
	Nonlinear form
Langmuir	$q_e = \frac{q_m K_L C_e}{1 + b C_e}$
Freundlich	$q_e = K_f C_e^{1/n}$
Temkin	$q_e = \frac{RT}{b} \ln A C_e$
Isotherm models	Three parameters
	Nonlinear form
Sips	$q_e = \frac{q_{ms}(K_S C_e)^{1/ns}}{1 + (K_S C_e)^{1/ns}}$
Toth	$q_e = \frac{q_{mT} C_e}{(1 + K_T C_e^{n_T})^{1/n_T}}$

$q_e$ : the amount of As(V) adsorbed per unit of adsorbent mass ( $\text{mg g}^{-1}$ );  $C_e$ : a concentration of adsorbate at equilibrium in the solution ( $\text{mg L}^{-1}$ );  $q_{(m,ms,mT)}$ : the maximum loading capacity ( $\text{mg g}^{-1}$ );  $K_L$ : the Langmuir constant ( $\text{L mg}^{-1}$ ) related to the energy of adsorption;  $K_f$ : Freundlich constants related to the adsorption capacity ( $\text{L mg}^{-1}$ );  $n$ : Freundlich constants related to the intensity, respectively;  $A$ : binding constant ( $\text{L g}^{-1}$ );  $b$ : Temkin constant;  $R$ : the universal gas constant ( $8.314 \text{ J mol}^{-1} \text{ K}^{-1}$ );  $T$ : the temperature at 298 K;  $K_S$ : the adsorption affinity;  $n_S$ : the system's heterogeneity;  $K_T$ : the adsorption affinity in Toth equation;  $n_T$ : the system heterogeneity in Toth equation

investigated by using  $2 \text{ g L}^{-1}$  of adsorbent dosage and  $10 \text{ mg L}^{-1}$  of As(V) concentration. In Fig. 7c, the results for Fe-Bent adsorbent showed the increase of As(V) adsorption percentage up to  $\text{pH}=8$ . However, the amount of As(V) removal in the Bent sample decreased at  $\text{pH}>4$ . Therefore, the different values of  $\text{pH}_{zpc}$  for Bent and Fe-Bent samples made different surface charge for As(V) adsorption in various pH. This suggested that the Fe-Bent was more capable than the Bent due to high positive surface charge for As(V) removal.

### 3.6 Sorption isotherms

The adsorption isotherm indicates how the adsorption molecules distribute between the liquid phase and the solid phase when the adsorption process reaches an equilibrium state. In this way, the two-parameter and three-parameter isotherm models were investigated to find the best fit for the experimental data. The distribution of As(V) onto the adsorption phase (Fe-Bent) was described well by Freundlich, Langmuir, Temkin (as two-parameter models), Sips and Toth models (as three-parameter models). The equations of all isotherm models are shown in Table 4.

The adsorption in the Langmuir isotherm model occurs on the homogeneous surface with monolayer formation without any interaction (Shaban et al. 2018). Freundlich isotherm model has been used for heterogeneous surface energy systems with the random distribution of sorption heat (Abukhadra et al. 2018a). The Temkin isotherm model has been used to investigate the indirect interactions among adsorbate–adsorbate and the heat of each molecule in each layer during the increase in surface coverage (Khalifa et al. 2016). The Temkin is one of the possible isotherm models to investigate the adsorption experimental data in contaminants and clay mineral system based on the chemisorption mechanism (Ahmedzeki et al. 2013).

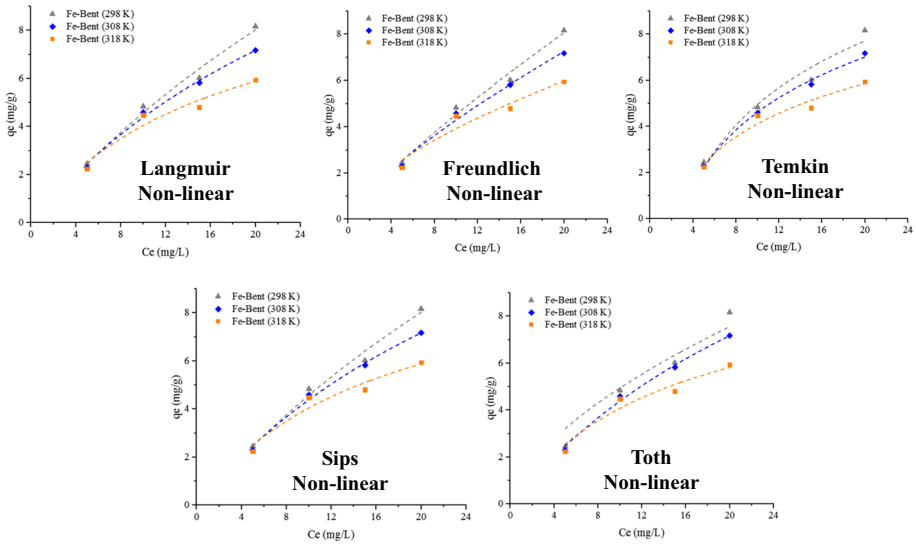


**Fig. 8** Two- and three-parameter isotherm models in nonlinear forms (at pH=10, adsorbent dosage = 2 g L<sup>-1</sup>, contact time=60 min and temperature of 298, 308 and 318 K)

Sips isotherm is the extended Langmuir–Freundlich model with a finite saturation capacity at high concentration (Ismadji et al. 2015). The heterogeneity parameter ( $n_s$ ) shows the behavior of Sips isotherm like as Freundlich model for  $n_s > 1$  and shows the behavior like as Langmuir for the value of  $n_s = 1$ . Toth isotherm model is the improved Henry law for low concentration without limitation in the saturation capacity for high concentration medium. This isotherm model showed multilayer and heterogeneous adsorption behaviors.

Figure 8 illustrates the isotherm models, and Table 5 shows the values of the isotherm constants, maximum adsorption capacities in Langmuir, Freundlich, Temkin, Sips and Toth models. The adsorption experimental data were fitted well to the Freundlich, Sips, Toth, Temkin and Langmuir isotherm models, respectively, due to the high values of  $R^2$  and the minimum amount of  $\chi^2$ . Following as Eqs. (4) and (5),  $R^2$  is the coefficient of determination in the range of 0–1 values, and  $\chi^2$  is the Chi-square tests used to estimate the best possible fit for the equilibrium model based on the optimal model (Markandeya and Kisku 2015).

$$R^2 = \frac{\sum_{i=1}^n (q_{(exp)} - q_{(cal)})^2}{\sum_{i=1}^n (q_{(exp)} - \overline{q_{(exp)}})^2} \tag{4}$$

$$\chi^2 = \sum_{i=1}^n \frac{(q_{(exp)} - q_{(cal)})^2}{q_{(exp),n}} \tag{5}$$

where  $q_{(exp)}$ ,  $\overline{q_{(exp)}}$ ,  $q_{(cal)}$  (mg g<sup>-1</sup>) are experimental, mean experimental, model predicted adsorption capacity amounts, and  $n$  is the number of data points. As shown in Fig. 8 and

**Table 5** The values of the isotherm constants, maximum adsorption capacities and error functions

Two parameters	Langmuir		Separation factor		Freundlich		Temkin					
	$q_m$ (mg g <sup>-1</sup> )	$K_L$ (L m g <sup>-1</sup> )	$R^2$	$R_L$	$k_f$ (L m g <sup>-1</sup> )	$n$	$R^2$	$\chi^2$	$b$	$A$	$R^2$	$\chi^2$
298 K	10.47	0.76	0.96	0.06–0.21	4.91	2.99	0.99	0.58	1347.32	16.48	0.97	0.71
308 K	7.96	1.14	0.99	0.04–0.15	4.43	3.73	0.99	0.12	1673.07	19.66	0.99	0.12
318 K	5.74	2.63	0.98	0.02–0.07	4.27	7.79	0.97	0.32	3676.31	40.18	0.97	0.31
Three parameters	Sips											
(K)	$q_{m1}$ (mg g <sup>-1</sup> )	$k_t$ (L m g <sup>-1</sup> )	$n_t$	$R^2$	$\chi^2$	$q_{ms}$ (mg g <sup>-1</sup> )	$K_s$ (L m g <sup>-1</sup> )	$n_s$	$R^2$	$\chi^2$		
298	10.26	1.04	0.03	0.98	1.12	10.06	1.18	2.72	0.98	0.17		
308	6.47	2.83	0.05	0.99	0.24	8.20	1.78	3.71	0.99	0.24		
318	5.85	3.29	0.87	0.99	0.62	5.75	2.53	1	0.99	0.61		

Table 5, the isotherm shape can be predicted using the dimensionless separation factor ( $R_L$ ) and the Freundlich exponent ( $1/n$ ). The  $R_L$  parameter is defined by Eq. (6).

$$R_L = \frac{1}{1 + K_L C_0} \quad (6)$$

where  $k_L$  is the Langmuir constant,  $C_0$  is the initial concentration ( $\text{mg L}^{-1}$ ).  $R_L$  was obtained from different ranges of initial concentrations. In this way,  $1/n > 1$  and  $R_L > 1$ ;  $1/n < 1$  and  $0 < R_L < 1$ ;  $1/n = 1$  and  $R_L = 1$  and  $1/n = 0$  and  $R_L = 0$  show the isotherm model is unfavorable, favorable, linear and irreversible, respectively (Kumar 2006; Tran et al. 2017). In this research, the obtained  $1/n$  and  $R_L$  values lower than 1 indicated that the As(V) adsorption onto Fe-Bent is favorable.

As shown in Fig. 8 and Table 5, the A values in Temkin model increased with increasing temperature indicated that the As(V) was better adsorbed on Fe-Bent with increasing temperature. Therefore, at a higher temperature, the increase in As(V) adsorption onto the Fe-Bent surface could be expected and the adsorption process was endothermic. The b values indicated the chemical interaction between As(V) and Fe-Bent (Erhayem et al. 2015). In Sips isotherm model,  $q_{ms}$  showed the maximum adsorption capacity similar to  $q_m$  in Langmuir model. Parameter  $n_s$  showed the behavior of Sips isotherm like as Freundlich model; however, the value of  $n_s = 1$  showed the homogeneous surface similar to Langmuir model in high temperature. According to the adsorption isotherm data, the heterogeneous surface sites mainly affected the As(V) adsorption.

To compare the adsorption capacity between Fe-Bent and the other clays/iron compounds, the physical properties (e.g., BET surface area, maximum adsorption capacity and iron content) and the experimental conditions (e.g., pH, adsorbent dosage and As(V) concentration) are evaluated in Table 6. The results showed that the Fe-Bent significantly improved the efficiency of As(V) adsorption.

### 3.7 Kinetic models of As(V) adsorption

In this research, the kinetic models of pseudo-first-order, pseudo-second-order and Elovich were investigated to describe the As(V) adsorption mechanism. All equations and parameters of these kinetic models are shown in Table 7. The plot of kinetic models is illustrated in Fig. 9. The pseudo-first-order model in many adsorption processes was found to be suitable for only a short time of interaction and not for the whole range of contact time. The pseudo-second-order model is based on a chemical adsorption reaction involving the valence forces through share or exchange of electrons between the adsorbent and the adsorbate (Mohan and Pittman 2007). Elovich equation has been used to describe the energetically heterogeneous nature of the adsorbent surface for chemisorption reactions (Shaban et al. 2017).

According to Table 8, the pseudo-second-order, Elovich and pseudo-first-order kinetic models were fitted well to the experimental kinetic data of Fe-Bent, respectively.

### 3.8 Adsorption thermodynamics

The thermodynamic adsorption parameters are calculated by Van't Hoff equation [Eq. (7)]:

$$\Delta G^0 = -RT \ln K_C \quad (7)$$

where  $K_C$  is the thermodynamic equilibrium constant,  $T$  is the solution temperature (K), and  $R$  is the universal constant ( $8.314 \text{ J mol}^{-1} \text{ K}^{-1}$ ).  $K_C$  represented the adsorption constant

**Table 6** Comparison between the adsorption capacity of Fe-Bent and the other clays/iron compounds

Adsorbent	pH	Temperature °C	As(V) concentration (mg L <sup>-1</sup> )	BET surface area (m <sup>2</sup> g <sup>-1</sup> )	Iron weight percent (wt%)	Maximum adsorption capacity (mg g <sup>-1</sup> )	References
Hematite	4.2	30	0.133	14.40	56.60	0.2	Singh et al. (1996)
Iron oxide-coated sand	7.6	22 ± 2	0.1	10.6	4.5	0.043	Thirunavukkarasu et al. (2003)
Montmorillonite	5	25	10–200	58	– 3.36	0.64	Mohapatra et al. (2007)
Fe (III)-modified natural zeolite	6–7	25	0.1–10	–	0.33	1.55	Stanić et al. (2009)
Bentonite	5	25	1–50	–	6.39	0.33	Mar et al. (2013)
Iron oxide	7	20	0.1–1	75.24	1.84	3.33	TC et al. (2017) and Prathna et al. (2018)
Iron oxide/alumina nanocomposites	7	20	0.1–1	–	–	2.5	
Fe-Bent	6	25	10	168	8.10	10.06	This study

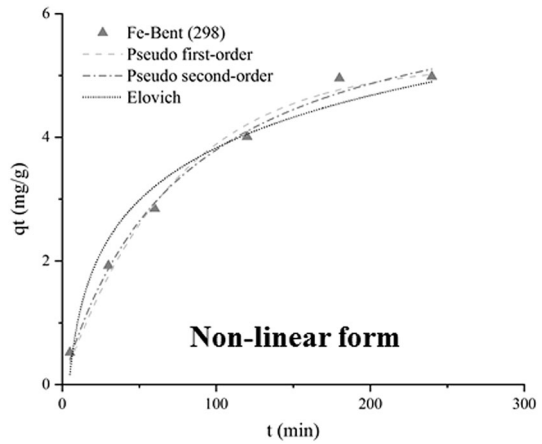


**Table 7** Equations and parameters of kinetic models

Kinetic models	Equations	Parameters
Pseudo-first-order	$q_t = q_e(1 - e^{-K_1 t})$	$q_e$ (mg g <sup>-1</sup> ) $K_1$ (min <sup>-1</sup> )
Pseudo-second-order	$q_t = \frac{q_e^2 K_2 t}{1 + q_e K_2 t}$	$q_e$ (mg g <sup>-1</sup> ) $K_2$ (g mg <sup>-1</sup> min <sup>-1</sup> )
Elovich	$q_t = \frac{1}{\beta} \ln(\alpha\beta) + \frac{1}{\beta} \ln(t)$	$\alpha$ (g mg <sup>-1</sup> min <sup>-1</sup> ) $\beta$ (mg g <sup>-1</sup> )

$q_e$ : the amounts of As(V) adsorbed at equilibrium time (mg g<sup>-1</sup>);  $q_t$ : the amounts of As(V) adsorbed at  $t$  (min) time (mg g<sup>-1</sup>);  $K_1$ : the rate constant in the pseudo-first-order adsorption (min<sup>-1</sup>);  $K_2$ : the rate constant in the pseudo-second-order adsorption (g mg<sup>-1</sup> min<sup>-1</sup>);  $\alpha$ : constants of the Elovich model corresponded to initial adsorption rate (mg g<sup>-1</sup> min<sup>-1</sup>);  $\beta$ : constants of the Elovich model corresponded to the surface coverage with the chemisorption activation energy (g mg<sup>-1</sup>)

**Fig. 9** Kinetic models in nonlinear forms (at pH=10, adsorbent dosage=2 g L<sup>-1</sup>, As(V) concentration=10 mg L<sup>-1</sup> and temperature of 298 K)



of the best isotherm model (Fenti et al. 2019; Tran et al. 2017). Therefore,  $K_f$  was selected for  $K_C$  determination due to the lowest  $\chi^2$  and highest  $R^2$  values (see Table 5). For the conversion of  $K_f$  Eq. (8) was used.

$$K_C = \frac{K_f \rho}{1000} \left( \frac{10^6}{\rho} \right)^{(1-1/n)} \tag{8}$$

where  $\rho$  is a density of pure water (assumed as ~1 g mL<sup>-1</sup>). Standard enthalpy  $\Delta H^0$  and standard entropy  $\Delta S^0$  were obtained by the plot of  $\ln K_C$  versus  $1/T$ . The standard free energy  $\Delta G^0$  was calculated from the Gibbs relation at a constant temperature [Eqs. (9) and (10)]:

$$\Delta G^0 = \Delta H^0 - T\Delta S^0 \tag{9}$$

$$\ln K_C = \frac{\Delta S^0}{R} - \frac{\Delta H^0}{RT} \tag{10}$$

**Table 8** Kinetic parameters and error functions

Sample	Pseudo-first-order			Pseudo-second-order			Elovich		
	$K_1$ ( $\text{min}^{-1}$ )	$q_{e(\text{cal})}$ ( $\text{mg g}^{-1}$ )	$R^2$	$K_2$ ( $\text{g mg}^{-1} \text{min}^{-1}$ )	$q_{e(\text{cal})}$ ( $\text{mg g}^{-1}$ )	$R^2$	$\alpha$ ( $\text{mg g}^{-1} \text{min}^{-1}$ )	$\beta$ ( $\text{mg g}^{-1}$ )	$\chi^2$
Fe-Bent	0.01	5.21	0.99	0.002	6.77	0.99	0.27	0.81	0.15

**Fig. 10** Van't Hoff plot of  $\ln K_e$  versus  $1/T$  for As(V) removal

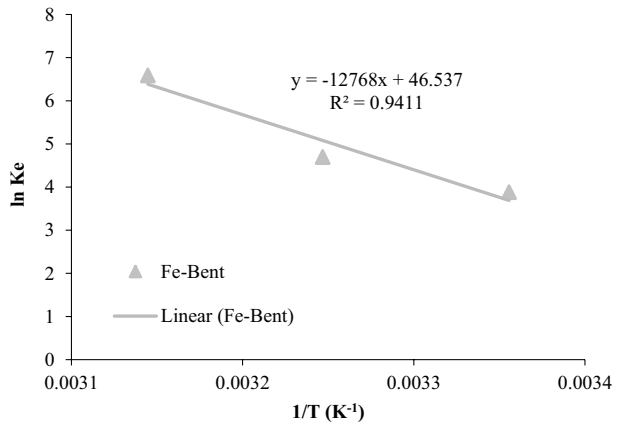


**Table 9** Thermodynamic parameters for sorption of As(V) on Fe-Bent

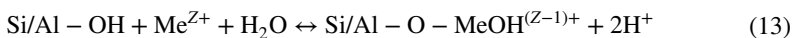
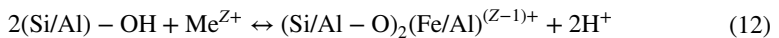
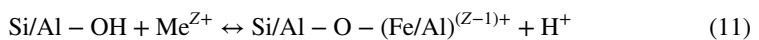
Temperature (K)	Thermodynamic parameters		
	$\Delta G^0$ (kJ mol <sup>-1</sup> )	$\Delta H^0$ (kJ mol <sup>-1</sup> )	$\Delta S^0$ (J mol <sup>-1</sup> K <sup>-1</sup> )
298	-9.61	106.15	386.91
308	-12.01		
318	-17.41		

where  $C_e$  is the equilibrium concentration of As(V) adsorbed on Fe-Bent (mg L<sup>-1</sup>) and  $C_0$  is the equilibrium concentration of As(V) in aqueous solution (mg L<sup>-1</sup>). The thermodynamic results are shown in Fig. 10 and Table 9. The obtained adsorption enthalpy ( $\Delta H^0 = 106.15$  kJ mol<sup>-1</sup>) for Fe-Bent represented the endothermic and chemical reaction. Therefore, it seems that the iron hydroxide groups kept the As(V) ions strongly. The spontaneity of the As(V) adsorption reaction onto Fe-Bent was exhibited by increasing temperature and decreasing  $\Delta G^0$ .

The experimental data with the investigation of isotherms, kinetic models and thermodynamic data suggested the following mechanism for As(V) adsorption on Fe-Bent:

Under acidic conditions (pH < pH<sub>zpc</sub>), the Fe-Bent surface is positively charged, and then, these positive charges are equaled to their accompanying anions. Therefore, the ligand exchange reactions happened and the present anionic species in the solution could be adsorbed. In this way, the complexation occurred on the surface of Fe-Bent with the interchange of the OH group in Fe-OH species [Eqs. (11)–(13)].

Moreover, the mechanism of As(V) adsorption in Fe-Bent strongly depends on the pH of the solution due to the formation of new sites with hydrated exchangeable metal cations on the surface (Ramstedt 2004).



## OH ligand interchange

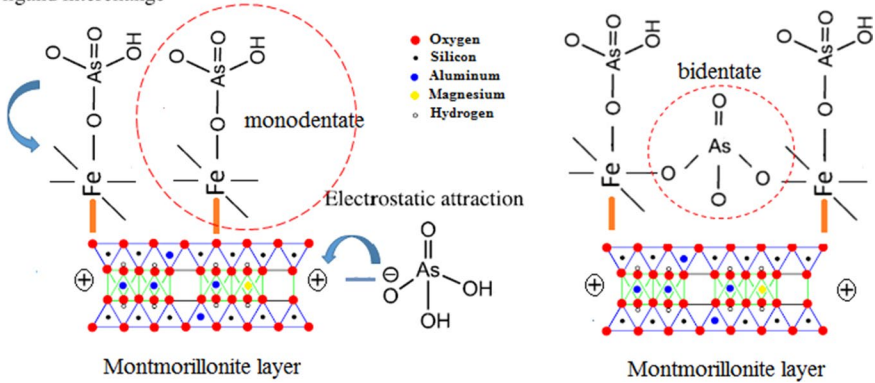
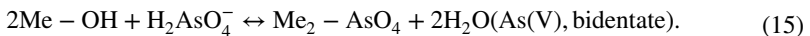


**Fig. 11** Adsorption mechanism of As(V) onto the montmorillonite layer of Fe-Bent

In Fe-Bent, the impregnated iron was mostly coordinated by various functional groups on bentonite. Moreover, the immobilization of As(V) species on the active sites of adsorbents was gained by Me–As surface complexes according to subsequent formulas [Eqs. (14) and (15)] (Doušová et al. 2009). At pH=6 (pH < pHzpc), the  $\text{H}_2\text{AsO}_4^-$  species was dominant. The adsorption mechanism of  $\text{H}_2\text{AsO}_4^-$  onto the Fe-Bent is shown in Fig. 11.



## 4 Conclusion

1. To increase the adsorption capacity of natural bentonite, the modification of bentonite surface is considered by the formation of isolated Fe(III) ions, small clusters and bulky  $\text{Fe}_x\text{O}_y$  particles in the porous structure of Bent.
2. Impregnation method made the crystalline and amorphous iron species in Fe-Bent, and improved bentonite porosity and surface area for As(V) adsorption.
3. The maximum As(V) adsorption for modified bentonite was determined in the rate of 99% (at adsorbent dosage =  $2 \text{ g L}^{-1}$ , As(V) concentration =  $10 \text{ mg L}^{-1}$  and pH = 6–8).
4. For a better understanding of As(V) adsorption, thermodynamics, kinetics and two-/three-parameter isotherm models were investigated. These isotherms, kinetics, thermodynamic models and the adsorption properties of Fe-Bent based on several analytical techniques confirmed that the sorption was chemical and endothermic.
5. The probable mechanisms of As(V) adsorption on Fe-Bent clay were the ligand exchange reactions and the inner-sphere complexation for the formation of stable and strong bidentate and monodentate As-Fe complexes.

**Acknowledgements** The authors acknowledge the support of Iranian nanotechnology initiative council (INIC) for providing the financial support to carry out this research with Grant Number 127212.

## References

- Abukhadra, M. R., Dardir, F. M., Shaban, M., Ahmed, E. A., & Soliman, M. F. (2018a). Superior removal of  $\text{Co}^{2+}$ ,  $\text{Cu}^{2+}$  and  $\text{Zn}^{2+}$  contaminants from water utilizing spongy Ni/Fe carbonate-fluorapatite; preparation, application and mechanism. *Ecotoxicology and Environmental Safety*, 157, 358–368.
- Abukhadra, M. R., Rabia, M., Shaban, M., & Verpoort, F. (2018b). Heulandite/polyaniline hybrid composite for efficient removal of acidic dye from water; kinetic, equilibrium studies and statistical optimization. *Advanced Powder Technology*, 29(10), 2501–2511.
- Ahmedzeki, N. S., Rashid, H. A., Alnaama, A. A., Alhasani, M. H., & Abdhussain, Z. (2013). Removal of 4-nitro-phenol from wastewater using synthetic zeolite and kaolin clay. *Korean Journal of Chemical Engineering*, 30(12), 2213–2218.
- Bower, C. A., Reitemeier, R., & Fireman, M. (1952). Exchangeable cation analysis of saline and alkali soils. *Soil Science*, 73(4), 251–262.
- Chen, L., Xin, H., Fang, Y., Zhang, C., Zhang, F., Cao, X., et al. (2014). Application of metal oxide heterostructures in arsenic removal from contaminated water. *Journal of Nanomaterials*, 2014, 2.
- Chibanal, M., Zerbet, M., Carja, G., & Sinan, F. (2012). Application of low-cost adsorbents for arsenic removal: A review. *Journal of Environmental Chemistry and Ecotoxicology*, 4(5), 91–102.
- Devi, R. R., Umlong, I. M., Das, B., Borah, K., Thakur, A. J., Raul, P. K., et al. (2014). Removal of iron and arsenic (III) from drinking water using iron oxide-coated sand and limestone. *Applied Water Science*, 4(2), 175–182.
- Doušová, B., Fuitová, L., Grygar, T., Machovič, V., Koloušek, D., Herzogová, L., et al. (2009). Modified aluminosilicates as low-cost sorbents of As (III) from anoxic groundwater. *Journal of Hazardous Materials*, 165(1), 134–140.
- Erhayem, M., Al-Tohami, F., Mohamed, R., & Ahmida, K. (2015). Isotherm, kinetic and thermodynamic studies for the sorption of mercury (II) onto activated carbon from *Rosmarinus officinalis* leaves. *American Journal of Analytical Chemistry*, 6(01), 1.
- Fazi, S., Amalfitano, S., Casentini, B., Davolos, D., Pietrangeli, B., Crognale, S., et al. (2016). Arsenic removal from naturally contaminated waters: A review of methods combining chemical and biological treatments. *Rendiconti Lincei*, 27(1), 51–58.
- Fenti, A., Iovino, P., & Salvestrini, S. (2019). Some remarks on “A critical review of the estimation of the thermodynamic parameters on adsorption equilibria. Wrong use of equilibrium constant in the Van’t Hoof equation for calculation of thermodynamic parameters of adsorption”. *Journal of Molecular Liquids*, 273, 425–434.
- Gitari, W. (2014). Attenuation of metal species in acidic solutions using bentonite clay: Implications for acid mine drainage remediation. *Toxicological and Environmental Chemistry*, 96(2), 201–217.
- Goldberg, S., & Johnston, C. T. (2001). Mechanisms of arsenic adsorption on amorphous oxides evaluated using macroscopic measurements, vibrational spectroscopy, and surface complexation modeling. *Journal of Colloid and Interface Science*, 234(1), 204–216.
- Ismadji, S., Soetaredjo, F. E., & Ayucitra, A. (2015). The kinetic studies in the adsorption of hazardous substances using clay minerals. In *Clay materials for environmental remediation*, Springer, pp. 113–120.
- Jovanović, B. M., Vukašinović-Pešić, V. L., Veljović, Đ. N., & Rajaković, L. V. (2011). Arsenic removal from water using low-cost adsorbents—A comparative study. *Journal of the Serbian Chemical Society*, 76(10), 1437–1452.
- Khalifa, L., Cervera, M. L., Bagane, M., & Souissi-Najar, S. (2016). Modeling of equilibrium isotherms and kinetic studies of Cr(VI) adsorption into natural and acid-activated clays. *Arabian Journal of Geosciences*, 9(1), 75.
- Krupskaya, V., Zakusin, S., Tyupina, E., Dorzhieva, O., Zhukhlistov, A., Belousov, P., et al. (2017). Experimental study of montmorillonite structure and transformation of its properties under treatment with inorganic acid solutions. *Minerals*, 7(4), 49.
- Kumar, K. V. (2006). Comments on “Adsorption of acid dye onto organobentonite”. *Journal of Hazardous Materials*, 137(1), 638–639.
- Langsch, J. E., Costa, M., Moore, L., Morais, P., Bellezza, A., & Falcão, S. (2012). New technology for arsenic removal from mining effluents. *Journal of Materials Research and Technology*, 1(3), 178–181.

- Liu, Y., Dong, C., Wei, H., Yuan, W., et al. (2015). Adsorption of levofloxacin onto an iron-pillared montmorillonite (clay mineral): Kinetics, equilibrium and mechanism. *Applied Clay Science*, *118*, 301–307.
- Lu, J. (1995). Comparative study on determination of iron contents in activated carbon. *Linchan Huaxue Yu Gongye*, *15*, 57–61.
- Mar, K., Karnawati, D., Putra, D., Igarashi, T., & Tabelin, C. (2013). Comparison of Arsenic adsorption on lignite, bentonite, shale, and iron sand from Indonesia. *Procedia Earth and Planetary Science*, *6*, 242–250.
- Markandeya, S., & Kisku, G. (2015). Linear and nonlinear kinetic modeling for adsorption of disperse dye in batch process. *Research Journal of Environmental Toxicology*, *9*, 320–331.
- Mohan, D., & Pittman, C. U. (2007). Arsenic removal from water/wastewater using adsorbents—A critical review. *Journal of Hazardous Materials*, *142*(1), 1–53. <https://doi.org/10.1016/j.jhazmat.2007.01.006>.
- Mohapatra, D., Mishra, D., Chaudhury, G. R., & Das, R. (2007). Arsenic (V) adsorption mechanism using kaolinite, montmorillonite and illite from aqueous medium. *Journal of Environmental Science and Health Part A*, *42*(4), 463–469.
- Nayak, P. S., & Singh, B. (2007). Instrumental characterization of clay by XRF, XRD and FTIR. *Bulletin of Materials Science*, *30*(3), 235–238.
- Oliveira, L. C., Rios, R. V., Fabris, J. D., Garg, V., Sapag, K., & Lago, R. M. (2002). Activated carbon/iron oxide magnetic composites for the adsorption of contaminants in water. *Carbon*, *40*(12), 2177–2183.
- Polowczyk, I., Cyganowski, P., Ulatowska, J., Sawiński, W., & Bastrzyk, A. (2018). Synthetic iron oxides for adsorptive removal of arsenic. *Water, Air, and Soil pollution*, *229*(6), 203.
- Pradisty, N. A., Sihombing, R., Howe, R. F., & Krisnandi, Y. K. (2017). Fe(III) oxide-modified Indonesian bentonite for catalytic photodegradation of phenol in water. *Makara Journal of Science*, *2017*, 25–33.
- Prathna, T., Sharma, S. K., & Kennedy, M. (2018). Application of iron oxide and iron oxide/alumina nanocomposites for arsenic and fluoride removal: A comparative study. *Journal of Theoretical and Applied Nanotechnology*, *6*.
- Prathna, T. C., Sharma, S. K., & Kennedy, M. (2017). Development of iron oxide nanoparticle adsorbents for arsenic and fluoride removal. *Desalination and Water Treatment*, *67*, 187–195.
- Putra, E. K., Pranowo, R., Sunarso, J., Indraswati, N., & Ismadji, S. (2009). Performance of activated carbon and bentonite for adsorption of amoxicillin from wastewater: Mechanisms, isotherms and kinetics. *Water Research*, *43*(9), 2419–2430.
- Ramstedt, M. (2004). *Chemical Processes at the Water-Manganite ( $\gamma$ -MnOOH) Interface*.
- Ranjan, D., Talat, M., & Hasan, S. (2009). Biosorption of arsenic from aqueous solution using agricultural residue 'rice polish'. *Journal of Hazardous Materials*, *166*(2), 1050–1059.
- Shaban, M., Abukhadra, M. R., Shahien, M., & Ibrahim, S. S. (2018). Novel bentonite/zeolite-NaP composite efficiently removes methylene blue and Congo red dyes. *Environmental Chemistry Letters*, *16*(1), 275–280.
- Shaban, M., Hassouna, M. E., Nasief, F. M., & AbuKhadra, M. R. (2017). Adsorption properties of kaolinite-based nanocomposites for Fe and Mn pollutants from aqueous solutions and raw ground water: Kinetics and equilibrium studies. *Environmental Science and Pollution Research*, *24*(29), 22954–22966.
- Sigdel, A., Park, J., Kwak, H., & Park, P.-K. (2016). Arsenic removal from aqueous solutions by adsorption onto hydrous iron oxide-impregnated alginate beads. *Journal of Industrial and Engineering Chemistry*, *35*, 277–286.
- Singh, D., Prasad, G., & Rupainwar, D. (1996). Adsorption technique for the treatment of As (V)-rich effluents. *Colloids and Surfaces A: Physicochemical and Engineering Aspects*, *111*(1–2), 49–56.
- Stanić, T., Daković, A., Živanović, A., Tomašević-Čanović, M., Dondur, V., & Miličević, S. (2009). Adsorption of arsenic (V) by iron (III)-modified natural zeolitic tuff. *Environmental Chemistry Letters*, *7*(2), 161–166.
- Thirunavukkarasu, O., Viraraghavan, T., & Subramanian, K. (2003). Arsenic removal from drinking water using iron oxide-coated sand. *Water, Air, and Soil pollution*, *142*(1–4), 95–111.
- Timofeeva, M., Khankhasaeva, S. T., Chesalov, Y. A., Tsybulya, S., Panchenko, V., & Dashinamzhilova, E. T. (2009). Synthesis of Fe, Al-pillared clays starting from the Al, Fe-polymeric precursor: Effect of synthesis parameters on textural and catalytic properties. *Applied Catalysis, B: Environmental*, *88*(1–2), 127–134.
- Tran, H. N., You, S.-J., Hosseini-Bandegharai, A., & Chao, H.-P. (2017). Mistakes and inconsistencies regarding adsorption of contaminants from aqueous solutions: A critical review. *Water Research*, *120*, 88–116.
- Türk, T., & Alp, I. (2014). Arsenic removal from aqueous solutions with Fe-hydroxalcite supported magnetite nanoparticle. *Journal of Industrial and Engineering Chemistry*, *20*(2), 732–738.

- Türk, T., Alp, İ., & Deveci, H. (2009). Adsorption of As(V) from water using Mg-Fe-based hydrotalcite (FeHT). *Journal of Hazardous Materials*, 171(1), 665–670. <https://doi.org/10.1016/j.jhazmat.2009.06.052>.
- Uddin, M. K. (2017). A review on the adsorption of heavy metals by clay minerals, with special focus on the past decade. *Chemical Engineering Journal*, 308, 438–462.
- Weber, W. J., Jr., & DiGianno, F. A. (1996). *Process dynamics in environmental systems*. New York: Wiley.
- Yamamura, S., Bartram, J., Csanady, M., Gorchev, H. G., & Redekopp, A. (2003). Drinking water guidelines and standards. *Arsenic, Water, and Health: The State of the Art*.
- Yan, L.-G., Shan, X.-Q., Wen, B., & Owens, G. (2008). Adsorption of cadmium onto Al 13-pillared acid-activated montmorillonite. *Journal of Hazardous Materials*, 156(1), 499–508.

**Publisher's Note** Springer Nature remains neutral with regard to jurisdictional claims in published maps and institutional affiliations.

## Affiliations

Shima Barakan<sup>1</sup> · Valeh Aghazadeh<sup>1</sup>  · Abdoullah Samiee Beyragh<sup>2</sup> · Sahar Mohammadi<sup>1</sup>

Shima Barakan  
shima.barakan@gmail.com

Abdoullah Samiee Beyragh  
samiee@acecr.ac.ir

Sahar Mohammadi  
sahar.m381@yahoo.com

<sup>1</sup> Department of Mineral Processing, Faculty of Mining Engineering, Sahand University of Technology, Tabriz, Iran

<sup>2</sup> Branch of Amirkabir, Iranian Academic Center for Education, Culture and Research (ACECR), Tehran, Iran